# Signature analysis of characteristic frequencies in a Francis turbine



IOP Conf. Series: Earth and Environmental Science **240** (2019) 072008 doi:10.1088/1755-1315/240/7/072008

# Signature analysis of characteristic frequencies in a Francis turbine

**Chirag Trivedi[1,*], Einar Agnalt[1], Ole Gunnar Dahlhaug[1] and Bard A Brandastro[1]**

[1]Department of Energy and Process Engineering, Faculty of Engineering, NTNU—Norwegian University of Science and Technology, Trondheim, 7491-Norway.

[*]E-mail: chirag.trivedi@ntnu.no

**Abstract**. The present work investigates the unsteady pressure fluctuations in a model Francis turbine that are observed during steady state operation. Focus of the present study is to correlate pressure fluctuations between stationary and rotating components in the turbine. It is challenging and expensive to perform pressure measurements inside the rotating parts of the turbine. Pressure measurements at the runner upstream and downstream can help to understand the signature of pressure pulsations in the blade passages. To this end, one pressure sensor in the vaneless space, four pressure sensors in the runner and two pressure sensors in the draft tube cone were integrated to acquire pressure data. Detailed analysis of the acquired pressure data is carried out including statistical analysis, spectral analysis and coherence analysis. Further, stochastic and deterministic analysis of the pressure fluctuations in the turbine is carried out. The results showed that pressure data in the vaneless space and the draft tube could be used to understand the signature of pressure fluctuations existed in the runner.

## 1. Introduction

Hydraulic turbines are designed for certain head and discharge conditions, where the efficiency is high, known as the best efficiency point (BEP) [1]. Rapid change of spot prices and the generation from the wind turbines often force turbines to operate at off-design conditions [2–4], starting from part load to the full load. This has resulted in increased cost of turbine operation and maintenance [5]. When a blade passes in front of a guide vane, it interacts and a momentum exchange between them takes place which develops waves. The interaction phenomenon is known as rotor-stator interaction (RSI). The stationary domains, distributor and draft tube, experience pressure fluctuations at a frequency ($f_b$) corresponding to the number of rotating blades ($z_b$) and rotational speed of the runner ($n$) as shown by equation (1). The rotating domain experience a frequency ($f_{gv}$) corresponding to the number of guide vanes ($z_{gv}$) and rotational speed of the runner ($n$) as shown by equation (2).

$$f_b = n \cdot z_b \quad (\mathrm{Hz}) \tag{1}$$

$$f_{gv} = n \cdot z_{gv} \quad (\mathrm{Hz}) \tag{2}$$

In a high-head Francis turbine, a gap (vaneless space) between the runner and the guide vane is small, and the pressure fluctuations associated with RSI are one of the key concerns. There have been several failures in hydraulic turbines, a majority of which pertained to RSI [6–8]. In the last two decades, several studies have been conducted on Francis turbines pertaining to RSI toward enabling safe prototype design [9,10]. In addition to RSI, stochastic pressure fluctuations are dominant at certain locations in the turbine

[11]. Dynamic characteristics of a turbine are determined through pressure (also strain) and velocity measurements at distinct locations in the turbine [12–14].

Majority of the pressure measurements are conducted in model turbines. The measurements are aimed to investigate the frequency spectra and the fatigue cycles on the blades. Some of the studies were focused on velocity measurements in the vaneless space and the draft tube [15]. Flow at runner downstream has relatively high circumferential velocity and intricate turbulence [16]. The vortex rope occurs typically at the part load condition, and the unsteady motion is associated with low frequency pressure pulsations. The vortex rope may have a frequency of $n/5$ to $n/3$ [17]. At part load, the vortex rope rotates in the same direction as the runner, whereas, at high load it rotates in opposite direction due to change in magnitude of swirl velocity leaving the runner [18]. There may be two types of pressure pulsations, synchronous and/or asynchronous type during turbine operation away from BEP [19]. As compared to the draft tube, very few velocity measurements are conducted in the vaneless space, and those were aimed to investigate the effect of rotating stall in pump-turbines [20]. Measurements on the prototype mainly focused on unsteady pressure loading in the turbine and vortex breakdown [21]. Measurements in the prototype runner are conducted for exceptional cases, such as refurbishment, validation of guaranteed parameters during commissioning of a turbine and in case of any premature failure/crack in the runner [22,23].

Three different approaches are used to determine dynamic characteristics of a turbine: (1) statistical analysis, (2) spectral analysis and (3) rainflow counting [24–26]. Statistical analysis allows to determine similarity between pressure measurement locations in the turbine. Amplitudes of specific frequencies at measurement locations are computed using spectral analysis. Furthermore, spectral analysis allows to estimate the power spectra of stochastic and deterministic signals as well as phase between specific frequencies. Rainflow counting is used to estimate the fatigue cycles for the given time and specified frequencies [27]. For example, speed-no-load conditions, unsteady pressure loading pertained to stochastic pressure fluctuations is dominant and cause heavy fatigue damage to blades. In this situation, rainflow counting is preferable to estimate the fatigue cycles. Unsteady pressure fluctuations are composed of deterministic, stochastic, synchronous and asynchronous type pulsations. Decomposition of such fluctuations can help to understand the similarity between the stationary and rotating domains.

Flow field either in the vaneless space or in the draft tube is affected by the flow field in the runner. Therefore, some extent it may be appropriate to assume that flow field in the vaneless space and the draft tube is representative of the flow field in the runner. Measurements in the stationary domains is not as expensive and time consuming as the measurements in the runner, mainly for prototype turbines. The present work aims to investigate unsteady pressure fluctuations in a model Francis turbine at three operating points, i.e., part load, BEP and high load. The focus is to analyze pressure data in the vaneless space, runner and draft tube, and to study the signature of pressure fluctuations at distinct locations in the turbine. Both statistical and spectral analysis is conducted to study common signature between pressure fluctuations in the stationary and rotating domains. Secondary objectives of the present study is: (1) How pressure fluctuations in the vaneless space and draft tube related to the pressure fluctuations in the runner and (2) Are pressure measurements in the stationary domains enough to predict pressure field in the runner.

## 2. Experimental setup

A model Francis turbine available in the Norwegian University of Science and Technology, was used for the measurements. Figure 1 shows the hydraulic loop of the test rig. Water from the large reservoir (9) was pumped to the overhead tank (2) and flowed down to the turbine (7). Hence, the volume flow rate to the turbine was regulated by the guide vanes. A feed pump (1) was operated at the selected speed to maintain constant head. The draft tube outlet was connected to a downstream tank (8), where a constant head was maintained at an atmospheric pressure and the water above the runner centerline was returned to the basement (9). The test rig is capable of producing head up to 16 m for the open loop and up to 100 m (discharge $\leq 0.5$ $m^3$ $s^{-1}$) for the closed loop. The open loop is used for the current measurements.

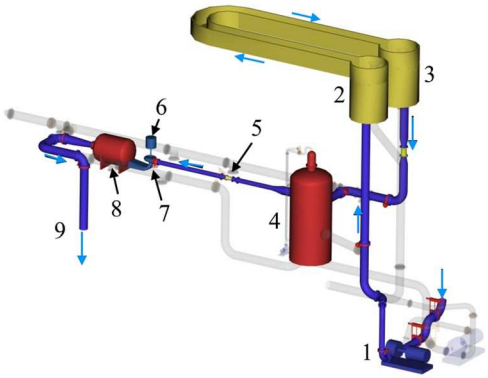


**Figure 1.** Open-loop hydraulic system of the model Francis turbine at the Waterpower Laboratory, NTNU. 1 – feed pump, 2 – overhead tank-primary, 3 – overhead tank-secondary, 4 – pressure tank, 5 – magnetic flowmeter, 6 – generator, 7 – Francis turbine, 8 – downstream tank and 9 – basement.

The turbine included 14 stay vanes integrated inside the spiral casing, 28 guide vanes, a runner with 15 blades and 15 splitters, and an elbow-type draft tube. The runner includes an alternating arrangement of a splitter and a blade. The runner inlet and outlet diameters were 0.63 m and 0.347 m, respectively. The turbine is equipped with standard instruments used to measure the head, discharge, torque, power, water temperature and rotational speed. The same instruments were used for the current study. An additional seven sensors were flush mounted to acquire pressure data from different locations. Sensor $V_1$ was located in the vaneless space. Four sensors ($R_1$, $R_2$, $R_3$ and $R_4$) were of the miniature type and were flush mounted to the surface of the runner crown in one blade channel. A slip-ring mechanism was used to transmit pressure data from the runner. Sensors $D_1$ and $D_2$ were located in the draft tube, 0.126 m downstream from the runner outlet and 180° circumferentially apart on the same plane. Pressure sensors in the runner are Entran and TE XP5 type, and the pressure measurement range was up to seven bar absolute. Uncertainty of the pressure sensor located in the vaneless space is 0.8% and in the runner is 0.2–1.2%.The natural frequencies of all the sensors were above 25 kHz, which is much higher than the maximum expected frequency in the test rig. Pressure data were acquired at a sampling rate of 10 kHz. The maximum expected frequency in the turbine is 1 kHz, i.e., the 5th harmonic of the blade passing frequency, which is much less than the sampling rate. Hence, the acquired pressure data will not be affected by the aliasing effect during data acquisition. Before the measurements, calibration and uncertainty quantification of all measuring instruments and sensors were performed. IEC 60193 was followed for quantifying the uncertainties. The total uncertainty ($\hat{e}_t$) of ±0.2% includes both systematic ($\hat{e}_s$) and random ($\hat{e}_r$) uncertainties.

$$\hat{e}_t = \pm\sqrt{\hat{e}_s^2 + \hat{e}_r^2} \tag{3}$$

The systematic uncertainty ($\hat{e}_s$) is the root-sum square of the uncertainties in the volume flow rate ($\hat{e}_Q$), head ($\hat{e}_H$), torque ($\hat{e}_T$), runner rotational speed ($\hat{e}_n$) and water density ($\hat{e}_\rho$) measurements. BEP was obtained at $\alpha$ = 9.9°, $n_{ED}$ = 0.18, and $Q_{ED}$ = 0.15, and the hydraulic efficiency was 93.1±0.2%. The volume flow rate to the turbine at BEP is 0.199 $m^3 s^{-1}$ ($Q_{ED}$ = 0.15), and the guide vane aperture is 100%. The runner was rotating at the synchronous speed, i.e., 5.55 revolutions per second.

## 3. Results and discussions

Experiments were conducted at three operating conditions, BEP, part load and high load. Detailed analysis of all pressure sensors and operating conditions have been carried out. Time dependent pressure fluctuations, power spectral density, coherence and signal-to-noise-ratio (SNR) of the acquired pressure data are studied in the stationary and rotating domains of the turbine. Unsteady pressure fluctuations in the vaneless space at BEP, part load and high load conditions are shown in figure 2. The pressure is normalized using equation (4), i.e. factor of pressure fluctuations ($\tilde{p}_E$).

$$\tilde{p}_{\mathrm{E}} = \frac{\tilde{p} - \bar{p}}{(\rho \cdot E)_{\mathrm{BEP}}} \tag{4}$$

where $\tilde{p}$ is the acquired pressure in Pascal, $\bar{p}$ is the average pressure in Pascal, $\rho$ is the water density in kg m$^{-3}$, and $E$ is the specific hydraulic energy in J kg$^{-1}$. The time of successive interactions between the blade and guide vane can be computed using equation (5).

$$t_{\mathrm{RSI}} = \frac{\left| z_{\mathrm{b}} - z_{\mathrm{gv}} \right|}{n \cdot z_{\mathrm{b}} \cdot z_{\mathrm{gv}}} \quad \text{(s)} \tag{5}$$

For the current turbine, time for the successive interaction is $4.29\times10^{-4}$ s, which is equivalent to 0.857° of angular rotation of the runner, and the RSI occurs in sequence as runner rotates. Furthermore, for the given combinations of guide vanes and blades including splitters, two guide vanes and two blade interact at same instant of time at exactly 180° circumferentially apart. Rotational speed of the runner and the frequencies are normalized using equation (6).

$$n^* = t \cdot n, \quad f^* = \frac{f}{n} \tag{6}$$

where $t$ is time in second, $f$ is frequency in Hz and $n$ is runner speed in revolutions per second. Pressure sensor $V_1$ shows pressure fluctuations in the vaneless space with respect to runner angular movement for one revolution. Pressure is high when the blade leading edge is in-front of the sensor $V_1$, and the pressure is low when two blade are equally apart from the sensor. Factor of pressure fluctuations is 2% of $\rho E$ for high load and the amplitudes of blade passing frequency ($f_b$) 0.3% of $\rho E$. Pressure data were acquired for 5 minutes and the spectral analysis was conducted using entire pressure signal.

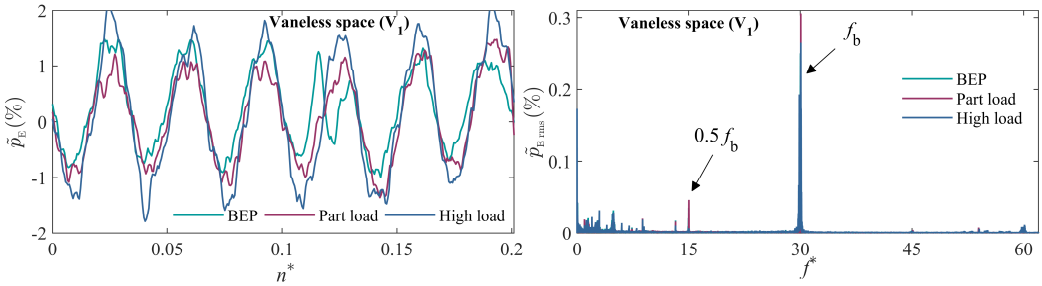


**Figure 2.** Pressure fluctuations and frequency spectra in the vaneless space ($V_1$) at BEP, part load and high load operating conditions.

Spectral analysis of unsteady pressure data at $R_1$ and $R_4$ locations for BEP, part load and high load conditions is shown in figure 3. High frequency stochastic fluctuations dominant at $R_4$ location as compared to the $R_1$. Two distinct frequencies, guide vane passing ($f_{gv}$) and the runner rotational speed ($f_n$) are obtained. Amplitudes of guide vane passing at part load and high load conditions are nearly same in the runner. The Amplitudes of RSI frequency are linearly decreasing along the blade channel. Stochastic fluctuations at $R_4$ location are visible due to strong influence of flow field from the draft tube. It can be seen that the amplitude of guide vane passing frequency at $R_1$ location is similar to the amplitude of blade passing frequency at $V_1$ location in the vaneless space. Pressure field in the vaneless space and the runner is largely driven by size and locations of the stagnation region at the guide vane trailing edge and the blade leading edge. Wake behind the guide vane is also influence the flow field, however, if the effect of stagnation pressure and size if strong, wake effect is almost negligible. For the present study, sensors are locations in the middle of the blade channel. A sensor on the blade leading edge, in the region of stagnation point, may show high amplitudes of RSI frequency. The sensor $V_1$ is located near the guide vane trailing edge where the amplitudes of RSI frequency are high as compared to other locations in the vaneless space. To study the pressure signal quality pertained to RSI and the stochastic (noise) fluctuations, SNR analysis is carried out.

$$\mathrm{SNR}_{\mathrm{dB}} = 10\log_{10}\left(\frac{P_{\mathrm{signal}}}{P_{\mathrm{stochastic\ noise}}}\right) \quad (\mathrm{dB}), \tag{7}$$

where $P$ is the power of the signal which is square of amplitude divided by two.

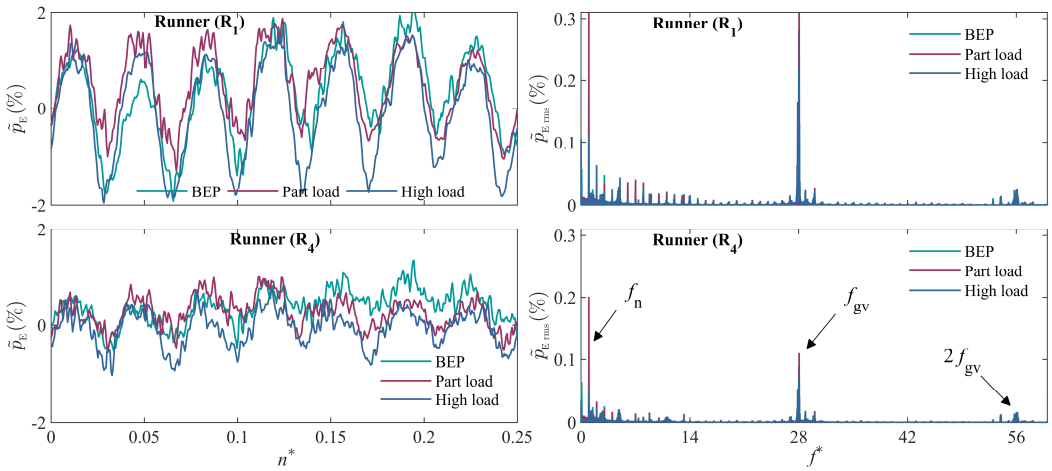


**Figure 3.** Pressure fluctuations and frequency spectra in the runner ($R_1$ and $R_4$) at BEP, part load and high load; $f_n$ is the frequency of runner speed and $f_{gv}$ is the frequency of guide vane passing.

Figure 4 shows SNR at all measurement locations in the turbine. Small difference in signal quality between $V_1$ and $R_1$ can be seen. Similarly, small difference between $R_4$ and $D_1$ can be seen. This indicates the random (including noise) fluctuations in the vaneless space and the runner are representative of runner up to certain extent. High load and part load show high value of SNR, which indicates the signal quality (amplitude) of $f_R$ and $f_{gv}$ is high with respect to noise content. To investigate in detail, coherence analysis of the pressure data is carried out. Figures 5 and 6 show coherence analysis of runner pressure sensors at part load and high load operating conditions. Interestingly, low frequency fluctuations show low coherence for both operating conditions. At part load, pressure fluctuations of high frequency (> 150 Hz) at $R_2$ and $R_3$ locations show high coherence, which indicates similar flow condition. However, $R_4$ shows very low coherence, which indicates rapid variation of flow field from $R_3$ to $R_4$. While comparing the coherence from part load to the high load operating condition, low coherence value $R_1$–$R_3$ to $R_1$–$R_4$ at variation of flow field from $R_2$ to $R_4$ is strong in case of high load. Unsteady pressure fluctuations at $R_2$ and $R_3$ locations show high coherence, whereas sensor $R_4$ shows coherence less than 0.5. This indicates the source for high frequency stochastic pressure fluctuations may be from the draft tube and not from the upstream of $R_4$.

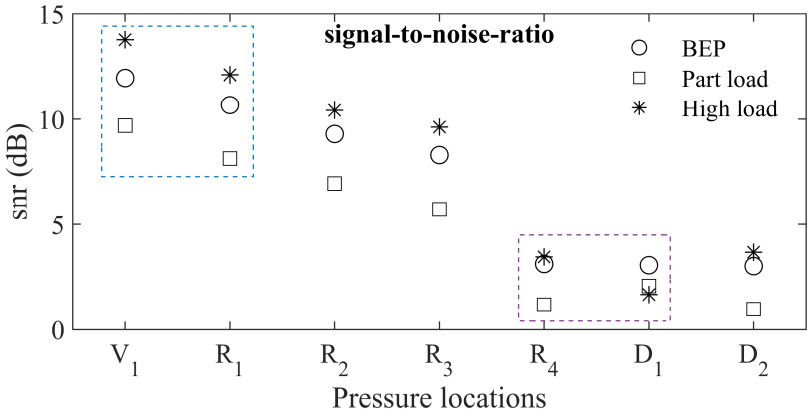


**Figure 4.** Signal-to-noise-ratio in the vaneless space, runner and draft tube at BEP, part load and high load.

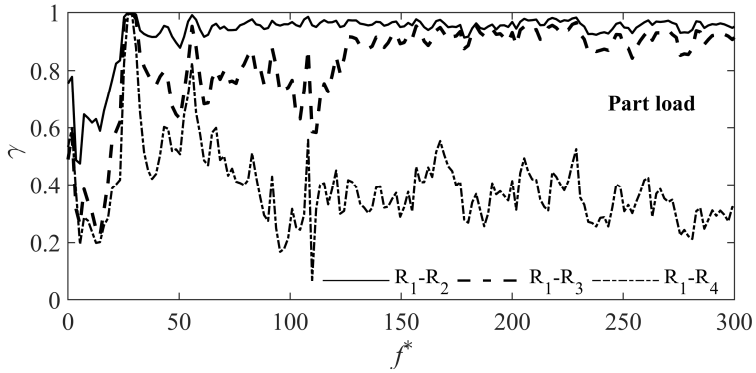


**Figure 5.** Coherence of pressure signals from runner locations at part load operating condition.

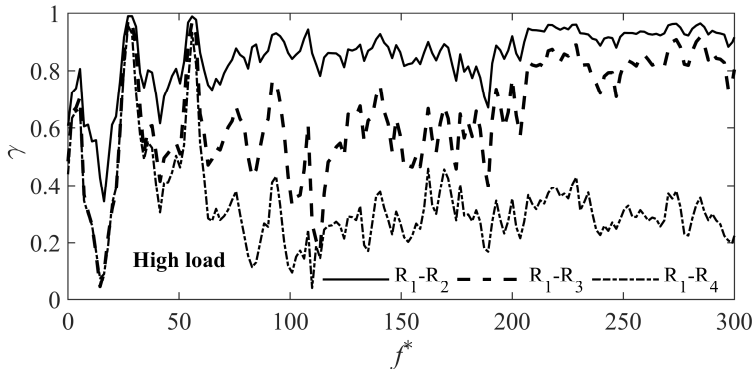


**Figure 6.** Coherence of pressure signals from runner locations at high load operating condition.

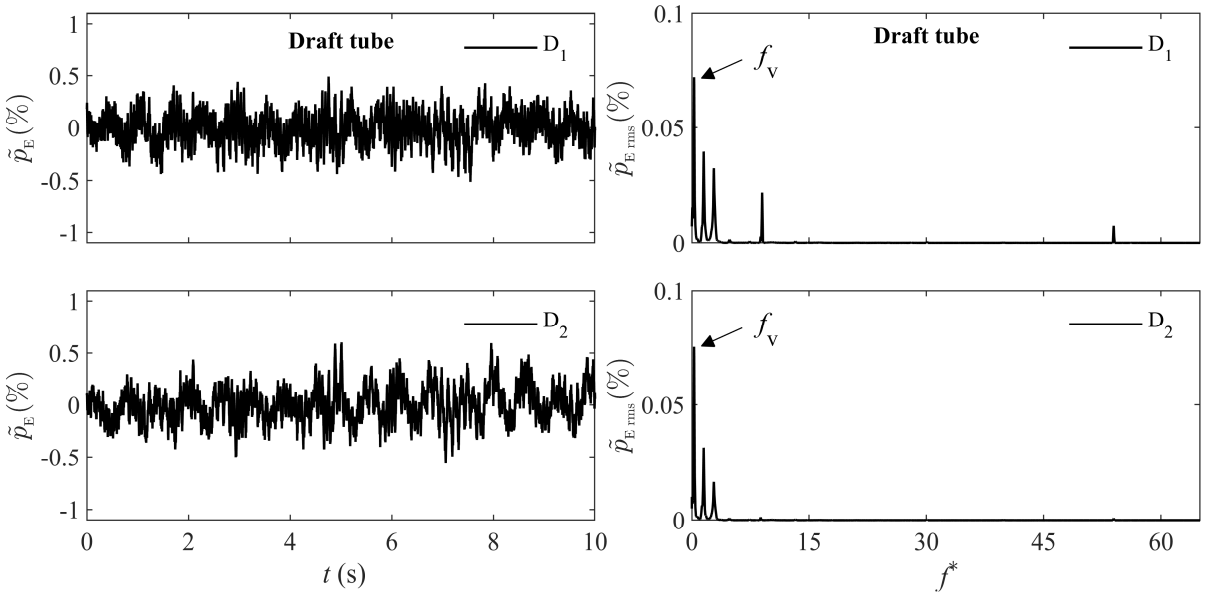


**Figure 7.** Pressure fluctuations and frequency spectra in the draft tube at part load operating condition; $f_v$ is the frequency of vortex rope.

In the draft tube, two pressure sensors $D_1$ and $D_2$ were mounted, and both were 180° circumferentially apart on the same plane. Figure 7 shows frequency spectra of pressure fluctuations from $D_1$ and $D_2$ locations in the draft tube. From the frequency spectra, high amplitudes of vortex rope frequency ($f_v$) and its harmonic are clearly visible. Two extra peaks at $D_1$, correspond to the frequency of supplied

power (50 Hz) and the DC generator (300 Hz). Amplitudes of blade passing frequency in the draft tube are very small (< 0.01% of $\rho E$). This has allowed to decompose pressure fluctuations related to synchronous and asynchronous type fluctuations in the draft tube. Coherence analysis at $D_1$ and $D_2$ locations showed very low coherence for the frequencies higher than 200 Hz. That indicates the random pressure fluctuations and there frequencies are different at both locations. The low frequency showed trend similar to $R_4$, especially 50–200 Hz, in figure 5. It is important to note that the sensor $R_4$ is in rotating domain therefore direct comparison is not accurate enough. However, the trend and frequencies can be useful to understand the local flow field at runner outlet. Overall, measurement in the draft tube can help to determine the stochastic fluctuations around blade trailing edge.

## 4. Conclusions

Unsteady pressure measurements were conducted on a model Francis turbine at three operating conditions, i.e., BEP, part load and high load. Total seven pressure sensors were integrated at different locations in the turbine. The present work is aimed to study common signature between pressure fluctuations in the stationary and rotating domains. Amplitude of RSI frequency were dominant at certain locations in the turbine; whereas, at other locations, amplitudes of stochastic pressure fluctuations were prevailing but smaller than the RSI frequencies. In the first half portion of blade channel, amplitudes of determinist frequencies were dominant. In the remaining position of the blade channel, especially after the trailing edge of splitter, stochastic pressure fluctuations were high. The source of stochastic fluctuations was unsteady vortex breakdown in the draft tube. Because, pressure sensors in the draft tube showed similar frequency band for the random fluctuations. Measurements in the draft tube, can provide information of the flow field in the runner up to some extent, especially random fluctuations. The draft tube pressure measurements could not provide the credible information on the RSI frequency because amplitudes of RSI frequencies in the draft tube were extremely small. From the draft tube pressure measurements, it is difficult to predict the deterministic frequency of RSI. From the present study, it may be concluded that the combined measurements in the vaneless space and the draft tube can provide information of pressure field in the blade channel up to some extent. In the first half part of the blade channel, deterministic frequencies prevail, which have signature similar to the frequencies in the vaneless space. In the second half part of the blade channel, stochastic frequencies prevail, which have signature similar to the draft tube flow condition.

## References

[1] Liu X, Luo Y, Karney B W and Wang W 2015 A selected literature review of efficiency improvements in hydraulic turbines *Renewable and Sustainable Energy Reviews* **51** pp 18–28. https://doi.org/10.1016/j.rser.2015.06.023.

[2] Beevers D, Branchini L, Orlandini V, De Pascale A and Perez-Blanco H 2015 Pumped hydro storage plants with improved operational flexibility using constant speed Francis runners *Applied Energy* **137** pp 629–637. https://doi.org/10.1016/j.apenergy.2014.09.065.

[3] Trivedi C, Agnalt E and Dahlhaug O G 2017 Investigations of unsteady pressure loading in a Francis turbine during variable-speed operation *Renewable Energy* **113** pp 397–410. https://doi.org/10.1016/j.renene.2017.06.005.

[4] Trivedi C, Agnalt E and Dahlhaug O G 2018 Experimental study of a Francis turbine under variable-speed and discharge conditions *Renewable Energy* **119** pp. 447–58. https://doi.org/10.1016/j.renene.2017.12.040.

[5] Monette C, Marmont H, Chamberland-Lauzon J, Skagerstrand A, Coutu A and Carlevi J 2016 Cost of enlarged operating zone for an existing Francis runner *IOP Conference Series: Earth and Environmental Science* **49** 072018. https://doi.org/10.1088/1755-1315/49/7/072018.

[6] Dorji U and Ghomashchi R 2014 Hydro turbine failure mechanisms: an overview *Engineering Failure Analysis* **44** pp 136–47. https://doi.org/10.1016/j.engfailanal.2014.04.013.

[7] Trivedi C 2017 A review on fluid structure interaction in hydraulic turbines: a focus on hydrodynamic damping *Engineering Failure Analysis* **77** pp 1–22. https://doi.org/10.1016/j.engfailanal.2017.02.021.
[8] Trivedi C and Cervantes M J 2017 Fluid structure interaction in hydraulic turbines: a perspective review *Renewable & Sustainable Energy Reviews* **68** pp 87–101. https://doi.org/10.1016/j.rser.2016.09.121.
[9] Zuo Z, Liu S, Sun Y and Wu Y 2015 Pressure fluctuations in the vaneless space of high-head pump-turbines-a review *Renewable and Sustainable Energy Reviews* **41** pp 965–74. https://doi.org/10.1016/j.rser.2014.09.011.
[10] Luna-Ramirez A, Campos-Amezcua A, Dorantes-Gomez O, Mazur-Czerwiec Z and Munoz-Quezada R 2016 Failure analysis of runner blades in a Francis hydraulic turbine - case study *Engineering Failure Analysis* **59** pp 314–25. https://doi.org/10.1016/j.engfailanal.2015.10.020.
[11] Kuibin P A, Shtork S I, Skripkin S G and Tsoy M A 2017 On random pressure pulses in the turbine draft tube *Journal of Physics: Conference Series* **813** 012051. https://doi.org/10.1088/1742-6596/813/1/01205.
[12] Nennemann B, Morissette J F, Chamberland-Lauzon J, Monette C, Braun O, Melot M, Coutu A, Nicolle J and Giroux A M 2014 Challenges in dynamic pressure and stress predictions at no-load operation in hydraulic turbines *IOP Conference Series: Earth and Environmental Science* **22** 032055. https://doi.org/10.1088/1755-1315/22/3/032055.
[13] Seidel U, Mende C, Hubner B, Weber W and Otto A 2014 Dynamic loads in Francis runners and their impact on fatigue life *IOP Conference Series: Earth and Environmental Science* **22** 032054. https://doi.org/10.1088/1755-1315/22/3/032054.
[14] Gagnon M, Tahan A, Bocher P and Thibault D 2014 Influence of load spectrum assumptions on the expected reliability of hydroelectric turbines: a case study *Structural Safety* **50** pp 1–8. https://doi.org/10.1016/j.strusafe.2014.03.008.
[15] Goyal R and Gandhi B K 2018 Review of hydrodynamics instabilities in Francis turbine during off-design and transient operations *Renewable Energy* **116** pp 697–709. https://doi.org/10.1016/j.renene.2017.10.012.
[16] Goyal R, Gandhi B K and Cervantes M J 2017 Experimental study of mitigation of a spiral vortex breakdown at high Reynolds number under an adverse pressure gradient *Physics of Fluids* **29** 104104. https://doi.org/10.1063/1.4999123.
[17] Trivedi C and Dahlhaug O G 2018 Interaction between trailing edge wake and vortex rings in a Francis turbine at runaway condition: Compressible large eddy simulation Physics of Fluids **30** 075101. https://doi.org/10.1063/1.5030867.
[18] Goyal R, Cervantes M J and Gandhi B K 2017 Vortex rope formation in a high head model Francis turbine *Journal of Fluids Engineering* **139** 041102. https://doi.org/10.1115/1.4035224.
[19] Amiri K, Cervantes M J and Mulu B 2015 Experimental investigation of the hydraulic loads on the runner of a Kaplan turbine model and the corresponding prototype *Journal of Hydraulic Research* **54** pp 1–14. https://doi.org/10.1080/00221686.2015.1040085.
[20] Goyal R, Gandhi B K and Cervantes M J 2018 PIV measurements in Francis turbine – a review and application to transient operations *Renewable and Sustainable Energy Reviews* **82** pp 1–16. https://doi.org/10.1016/j.rser.2017.06.108.
[21] Li Z, Wang Z, Wei X and Qin D 2016 Flow similarity in the rotor-stator interaction affected region in prototype and model pump-turbines *Journal of Fluids Engineering* **138** 061201. https://doi.org/10.1115/1.4032298.
[22] Trivedi C, Gogstad P J and Dahlhaug O G 2018 Investigation of the unsteady pressure pulsations in the prototype Francis turbines -part 1: steady state operating conditions *Mechanical Systems and Signal Processing* **108** pp 188–202. https://doi.org/10.1016/j.ymssp.2018.02.007.

[23] Huang X, Chamberland-Lauzon J, Oram C, Klopfer A and Ruchonnet N 2014 Fatigue analyses of the prototype Francis runners based on site measurements and simulations *IOP Conference Series: Earth and Environmental Science* **22** 012014. https://doi.org/10.1088/1755-1315/22/1/012014.
[24] Mende C, Weber W and Seidel U 2016 Progress in load prediction for speed-no-load operation in Francis turbines *IOP Conference Series: Earth and Environmental Science* **49** 062017. https://doi.org/10.1088/1755-1315/49/6/062017.
[25] Morissette J, Chamberland-Lauzon J, Nennemann B, Monette C, Giroux A, Coutu A and Nicolle J 2016 Stress predictions in a Francis turbine at no-load operating regime *IOP Conference Series: Earth and Environmental Science* **49** 072016. https://doi.org/10.1088/1755-1315/49/7/072016.
[26] Doerfler P and Ruchonnet N 2012 A statistical method for draft tube pressure pulsation analysis *IOP Conference Series: Earth and Environmental Science* **15** 062002. https://doi.org/10.1088/1755-1315/15/6/062002.
[27] Liu X, Luo Y and Wang Z 2016 A review on fatigue damage mechanism in hydro turbines *Renewable and Sustainable Energy Reviews* **54** 1–14. https://doi.org/10.1016/j.rser.2015.09.025.